Microfluid Nanofluid (2014) 17:1095–1104
DOI 10.1007/s10404-014-1397-8

RESEARCH PAPER

Isothermal flows of rarefied ternary gas mixtures in long tubes

Lajos Szalmas

Received: 1 January 2014 / Accepted: 3 April 2014 / Published online: 20 April 2014

Abstract A method is presented to determine isothermal flows of three-component rarefied gaseous mixtures in long tubes. The flow is subject to arbitrary but small local density gradients, when linearization can be applied. The mixture is described by the McCormack kinetic model, which is solved by discretizing the spatial and velocity spaces. Results are presented for the realistic and hard-sphere molecular interactions. The dimensionless kinetic coefficients are presented and commented for He–Ar–Xe mixture in a wide range of the rarefaction and numerous values of the mole fractions. The velocity profiles of the components are also shown. An additional method is also developed to solve the flow problem of the mixture driven by a global pressure difference between the two ends of the tube. The flow rates and the distributions of the mole fractions and the pressure along the axis of the tube are presented for pressure-driven flows of He–Ar–Xe mixture. The flow of the ternary mixture exhibits the separation phenomenon. The profiles of the mole fractions are non-uniform.

Keywords Ternary gas mixture · McCormack kinetic model · Discrete velocity calculation · Pressure-driven flow · Gaseous separation

1 Introduction

Flows of rarefied gases through long channels have great scientific importance. The analysis of these flows has recently received significant attention, which is well justified by the appearance of gaseous micro- and nanoflows and the revival of conventional applications in vacuum technology (Kandlikar and Garimella 2006; Li 2008; Jousten 2008; Sharipov 2013). When the mean-free path of the molecules becomes comparable with the characteristic length of the flow, the description should be based on the kinetic level valid in the whole range of the gaseous rarefaction (Cercignani 2006).

Previous numerical works have focused on the solution of linearized kinetic equations by using deterministic or probabilistic methods. For gaseous mixtures, more flow parameters are involved in the description. The molecular interactions can be defined by the original Boltzmann equation or kinetic models. For computational perspectives, the application of kinetic models is more straightforward since their numerical solution requires less computational effort. Among various approaches, e.g., Sirovich (1962), Morse (1964), Andries et al. (2002), McCormack (1973), the McCormack linearized kinetic model (McCormack 1973) seems the most suitable for the representation of gaseous mixtures. All transport coefficients in the model can be adjusted to arbitrary values; hence, the transport processes of the mixture can accurately be described. The McCormack kinetic model for binary gases has been solved by using the discrete velocity method for flows between two parallel plates (Naris et al. 2004b) and through long channels with rectangular (Naris et al. 2004a), circular (Sharipov and Kalempa 2002; Szalmas 2013a), triangular, and trapezoidal (Szalmas and Valougeorgis 2010) cross sections. The predictions of the model have been validated against the experimental measurement of the flow rate of He–Ar gas mixture for pressure-driven flows (Szalmas et al. 2010). The comparative study yielded good agreement between the theoretical and experimental flow rates. The model has also

L. Szalmas (✉)
Center for Environmental Research and Sustainable Technology, University of Bremen, Bremen, Germany
e-mail: lszalmas@gmail.com

been solved by using the probabilistic variance-reduced direct simulation Monte Carlo for various flow configurations (Szalmas 2012, 2013b). The flows of gaseous mixtures in channels are affected by the separation phenomenon (Sharipov and Kalempa 2005; Szalmas and Valougeorgis 2010; Szalmas et al. 2010; Szalmas 2010). At finite rarefaction, the number of molecular collisions is reduced, and the different species acquire different macroscopic speeds, resulting into the non-uniformity of the mole fractions of the components. All previous works have referred to binary gases, and practically, there is no similar work for mixtures with more components. However, multi-component gases can appear in applications and can exhibit interesting physical phenomena. For this reason, it is useful to consider such flows as well.

The goal of this paper is to determine isothermal flows of ternary gaseous mixtures through long tubes. The most general case is considered when arbitrary local density gradients are present in the gas. The McCormack kinetic model is used to describe the three-component gaseous mixture. A methodology is developed to solve the model and calculate the so-called kinetic coefficients. Results are delivered in terms of the kinetic coefficients and the velocity profiles for a selected He–Ar–Xe mixture in a wide range of gaseous rarefaction and various values of the mole fractions. Furthermore, a method is presented to calculate the properties of a global pressure-driven flow in a long tube. The component flow rates and the distributions of the mole fractions and the pressure of He–Ar–Xe mixture are shown and commented on.

2 Definition of the problem

The flow of a ternary gas mixture through a cylindrical tube under isothermal condition is considered. The radius and the length of the tube are denoted by R and L. It is assumed that the tube is long $R \ll L$. The axis of the channel is along the z' Cartesian coordinate direction, while its cross section is located in the (x', y') coordinate sheet. The problem has axial symmetry. The radial coordinate in the cross section is also introduced as r'. The mixture consists of three components, $\alpha = 1, 2, 3$. The number density and the molecular mass of the species are given by n_α and m_α. The mole fraction of each species is introduced as $C_\alpha = n_\alpha/n$, where $n = \sum_\alpha n_\alpha$ is the total density.

The gaseous mixture is characterized by the rarefaction parameter

$$\delta = \frac{PR}{\mu v_0}, \tag{1}$$

where P is the total pressure, μ is the viscosity, and $v_0 = \sqrt{2k_B T/m}$ is the characteristic molecular speed. Here, k_B, T are the Boltzmann constant and the temperature, and $m = \sum_\alpha C_\alpha m_\alpha$ is the average mass of the mixture.

It is supposed that the gas is subject to the following local dimensionless density gradients

$$X_\alpha = \frac{\partial n_\alpha}{\partial z'} \frac{R}{n_\alpha}. \tag{2}$$

The main interest of this work is in the particle fluxes of the species defined by

$$J'_\alpha = 2\pi \int_0^R n_\alpha u'_{\alpha z}(r') r' \mathrm{d}r', \tag{3}$$

where $u'_{\alpha z}(r')$ is the axial component of the velocity of species α.

Since the channel is long, the speed of the flow is small, and a linearized description can be used. In this work, the most general case when all possible driving terms are present is considered. The particle flux is a linear function of the density gradients

$$J'_\alpha = -\sum_{\beta=1}^{3} L'_{\alpha\beta} X_\beta, \tag{4}$$

where $L'_{\alpha\beta}$ are the generalized kinetic coefficients. It is noted that the elements of $L'_{\alpha\beta}$ are subject to the Onsager relation, $L'_{\alpha\beta} = L'_{\beta\alpha}$ (Sharipov 1994). The dimensionless kinetic coefficients are introduced according to

$$L_{\alpha\beta} = \frac{2}{n_\alpha A v_0} L'_{\alpha\beta}, \tag{5}$$

where $A = R^2\pi$ is the area of the cross section.

The primary goal of this work is to calculate the dimensionless kinetic coefficients $L_{\alpha\beta}$. If these coefficients are known, the local flow can be deduced for all possible values of the driving forces X_α due to the linear description. In addition, the flow rates and the distributions of the mole fractions and the pressure for global pressure-driven flows of the ternary mixture are calculated. This calculation is based on the precomputed kinetic coefficients and the consideration of the conservation of the mass along the axis of the channel.

3 Method of solution

3.1 The McCormack model

The local flow problem is solved at the kinetic level by utilizing the McCormack kinetic equation. Such a description is valid in the whole range of the gaseous rarefaction. The McCormack model consists of a free relaxation term and a third-order polynomial source term (McCormack 1973). The coefficients of the polynomial are

related to the Chapman–Cowling integrals, which ensure the correct transport properties in the hydrodynamic limit.

The gas is described by the velocity distribution function $f_\alpha(\boldsymbol{v}, r', z')$ with $\boldsymbol{v}$ denoting the microscopic velocity. This function is linearized according to

$$f_\alpha(\boldsymbol{v}, r', z') = f_\alpha^{(0)}(\boldsymbol{v}, z')[1 + h_\alpha(\boldsymbol{v}, r')], \tag{6}$$

where $h_\alpha(\boldsymbol{v}, r')$ is the perturbation function and

$$f_\alpha^{(0)}(\boldsymbol{v}, z') = n_\alpha(z')\pi^{-3/2} v_{0\alpha}^{-3} e^{-v^2/v_{0\alpha}^2} \tag{7}$$

is the local equilibrium distribution with $v_{0\alpha} = \sqrt{2k_B T/m_\alpha}$.

Dimensionless coordinates and velocity variables are introduced according to $r = r'/R$, $z = z'/R$ and $\boldsymbol{c}_\alpha = \boldsymbol{v}/v_{0\alpha}$. The cylindrical representation of the dimensionless molecular velocity $(c_{\alpha r}, \varphi, c_{\alpha z})$ is defined by $c_{\alpha x} = c_{\alpha r}\cos(\varphi)$ and $c_{\alpha y} = c_{\alpha r}\sin(\varphi)$.

By using the new coordinates, the McCormack kinetic equation for the three-component gas mixture and the cylindrical geometry reads such that

$$c_{\alpha x}\frac{\partial h_\alpha}{\partial r} - \frac{c_{\alpha y}}{r}\frac{\partial h_\alpha}{\partial \varphi} = \omega_\alpha \sum_{\beta=1}^{3} Q_{\alpha\beta} - X_\alpha c_{\alpha z}, \tag{8}$$

where $\omega_\alpha = R/v_{0\alpha}$ and

$$\begin{aligned} Q_{\alpha\beta} = {} & -\gamma_{\alpha\beta}h_\alpha + 2\left(\frac{m_\alpha}{m}\right)^{1/2} A_{\alpha\beta}c_{\alpha z} + 4B_{\alpha\beta}c_{\alpha x}c_{\alpha z} \\ & + \frac{4}{5}\left(\frac{m_\alpha}{m}\right)^{1/2} D_{\alpha\beta}c_{\alpha z}\left(c_\alpha^2 - \frac{5}{2}\right) \end{aligned} \tag{9}$$

is the collision term. Here, the coefficients $A_{\alpha\beta}$, $B_{\alpha\beta}$, $D_{\alpha\beta}$ are given by

$$\begin{aligned} A_{\alpha\beta} &= \gamma_{\alpha\beta}u_{\alpha z} - v_{\alpha\beta}^{(1)}(u_{\alpha z} - u_{\beta z}) - \frac{1}{2}v_{\alpha\beta}^{(2)}\left(q_{\alpha z} - \frac{m_\alpha}{m_\beta}q_{\beta z}\right), \\ B_{\alpha\beta} &= (\gamma_{\alpha\beta} - v_{\alpha\beta}^{(3)})p_{\alpha xz} + v_{\alpha\beta}^{(4)}p_{\beta xz}, \\ D_{\alpha\beta} &= (\gamma_{\alpha\beta} - v_{\alpha\beta}^{(5)})q_{\alpha z} + v_{\alpha\beta}^{(6)}\left(\frac{m_\beta}{m_\alpha}\right)^{1/2} q_{\beta z} - \frac{5}{4}v_{\alpha\beta}^{(2)}(u_{\alpha z} - u_{\beta z}), \end{aligned} \tag{10}$$

where $\gamma_{\alpha\beta}$, $v_{\alpha\beta}^{(k)}$ are the collision frequencies. The relevant macroscopic moments, the dimensionless axial velocity, shear stress, and axial heat flux are defined by

$$u_{\alpha z} = \left(\frac{m}{m_\alpha}\right)^{1/2}\pi^{-3/2}\int h_\alpha c_{\alpha z}e^{-c_\alpha^2}\mathrm{d}\boldsymbol{c}_\alpha, \tag{11}$$

$$p_{\alpha xz} = \pi^{-3/2}\int h_\alpha c_{\alpha x}c_{\alpha z}e^{-c_\alpha^2}\mathrm{d}\boldsymbol{c}_\alpha, \tag{12}$$

$$q_{\alpha z} = \left(\frac{m}{m_\alpha}\right)^{1/2}\pi^{-3/2}\int h_\alpha c_{\alpha z}\left(c_\alpha^2 - \frac{5}{2}\right)e^{-c_\alpha^2}\mathrm{d}\boldsymbol{c}_\alpha. \tag{13}$$

It is emphasized that Eq. (8) represents a system of three equations, $\alpha = 1, 2, 3$. Each equation is for one of the three components. The driving term X_α is a three-component vector. Each component of X_α stands for the dimensionless density gradient of the corresponding gaseous species. At the tube wall, the diffuse reflection boundary condition is assumed for the reflected molecules $h_\alpha(\boldsymbol{c}_\alpha, 1) = 0$ for $c_{\alpha x} < 0$.

The dimensionless kinetic coefficients can be deduced as

$$L_{\alpha\beta} = 4\int_0^1 u_{\alpha z}(r) r\mathrm{d}r \tag{14}$$

with the driving force $X_\eta = -E_{\eta\beta}$, where $\eta = [1, 2, 3]$ and $E_{\eta\beta}$ is the eigenmatrix. As indicated, the determination of the kinetic coefficients requires three different calculations, each one with different $X_\eta = -E_{\eta\beta}$. On the basis of the outcome of these calculations, the macroscopic quantities for an arbitrary driving term X_β can also be deduced by the following linear decomposition

$$u_{\alpha z} = -\sum_{\beta=1}^{3} u_{\alpha z}^{(\beta)}X_\beta,\ p_{\alpha xz} = -\sum_{\beta=1}^{3} p_{\alpha xz}^{(\beta)}X_\beta,\ q_{\alpha z} = -\sum_{\beta=1}^{3} q_{\alpha z}^{(\beta)}X_\beta, \tag{15}$$

where $u_{\alpha z}^{(\beta)}$, $p_{\alpha xz}^{(\beta)}$ and $q_{\alpha z}^{(\beta)}$ are the macroscopic quantities for $X_\eta = -E_{\eta\beta}$. It is noted that $u_{\alpha z}^{(\beta)}, p_{\alpha xz}^{(\beta)}, q_{\alpha z}^{(\beta)}$ formally are the macroscopic quantities for the perturbation functions $h_\alpha^{(\beta)}$ defined by the decomposition $h_\alpha = \sum_{\beta=1}^{3} h_\alpha^{(\beta)}X_\beta$. However, the introduction of $h_\alpha^{(\beta)}$ is not needed in the present formalism since $u_{\alpha z}^{(\beta)}, p_{\alpha xz}^{(\beta)}, q_{\alpha z}^{(\beta)}$ are defined by setting $X_\eta = -E_{\eta\beta}$.

For the free molecular limit, $\delta = 0$, an explicit analytical expression for the dimensionless kinetic coefficients can be obtained. In this situation, there is no exchange of moments among the species. For pressure-driven flows, the free molecular flow rates for single gases and binary mixtures have been determined by many authors (see, e.g., Sharipov and Kalempa 2002). For the present ternary mixture, the kinetic coefficients in the free molecular limit are given by

$$L_{\alpha\alpha} = \frac{8}{3\sqrt{\pi}}\sqrt{\frac{m}{m_\alpha}} \tag{16}$$

and $L_{\alpha\beta} = 0$ for $\alpha \neq \beta$.

3.2 Viscosity function

In order to define the model, the collision frequencies and the quantity ω_α are to be determined. The collision frequencies $v_{\alpha\beta}^{(k)}$ can be deduced by assuming a particular interaction among the molecules. They are the functions of the Chapman–Cowling integrals. The explicit expression of

$\nu_{\alpha\beta}^{(k)}$ can be found in Szalmas (2010) for example. Typically, $\nu_{\alpha\beta}^{(k)}$ are calculated in an arbitrary unit. Hence, after the collision frequencies are set, ω_α is to be deduced in order to obtain the proper normalization and connect the collision frequencies to the rarefaction parameter.

To find ω_α, the viscosity of the model is calculated. This is not a trivial task for a three-component mixture, but for the McCormack model the mixture viscosity can be determined exactly. Let us assume a plane shear flow along the axial direction. For a while, imagine that the flow varies only in the coordinate direction x'. On the basis of the global shear flow, the viscosity is defined by

$$P_{xz} = -\frac{PH}{\delta_H v_0}\frac{\partial u_z'}{\partial x'} = -\mu\frac{\partial u_z'}{\partial x'}, \tag{17}$$

where P_{xz} is the dimensional shear stress, u_z' is the axial velocity of the mixture, H is the characteristic length, and δ_H is the rarefaction parameter on the basis of H. The shear stress can be expressed as $P_{xz} = 2P\sum_\alpha C_\alpha p_{\alpha xz}$. Hence, the viscosity can be obtained by

$$\mu\frac{\partial u_z'}{\partial x'} = -2P\sum_{\alpha=1}^{3} C_\alpha p_{\alpha xz}. \tag{18}$$

For the uniform shear flow, the McCormack model with three components is analytically solvable. In this case, the second derivative on the left-hand side of Eq. (8) is omitted, $X_\alpha = 0$ and $R = H$. The solution yields that the viscosity can be written by

$$\mu = P\sum_{\alpha=1}^{3} C_\alpha\hat{\mu}_\alpha, \tag{19}$$

where $\hat{\mu}_\alpha$ is the solution of the following system of linear equations with three unknowns

$$\Phi_\alpha\hat{\mu}_\alpha - \nu_{\alpha\beta}^{(4)}\hat{\mu}_\beta - \nu_{\alpha\eta}^{(4)}\hat{\mu}_\eta = 1 \tag{20}$$

with $\Phi_\alpha = \nu_{\alpha\alpha}^{(3)} + \nu_{\alpha\beta}^{(3)} + \nu_{\alpha\eta}^{(3)} - \nu_{\alpha\alpha}^{(4)}$ and $\alpha,\beta,\eta = [1,2,3]$, $\alpha\neq\beta\neq\eta\neq\alpha$. Equation (20) is analytically solved to obtain $\hat{\mu}_\alpha$.

In the kinetic equation, the quantity $\gamma_{\alpha\beta}$ appears in the combination $\gamma_\alpha := \gamma_{\alpha\alpha} + \gamma_{\alpha\beta} + \gamma_{\alpha\eta}$, which is chosen in order to cover the correct relaxation for a single gas $\gamma_\alpha = 1/\hat{\mu}_\alpha$. Finally, ω_α is defined such that

$$\omega_\alpha = \delta\left(\frac{m_\alpha}{m}\right)^{1/2}\sum_{\alpha=1}^{3} C_\alpha\hat{\mu}_\alpha. \tag{21}$$

3.3 Numerical scheme

The description of the problem can be simplified by introducing the following reduced distribution function

$$Y_\alpha^{(k)}(c_{\alpha x}, c_{\alpha y}, r) = \pi^{-1/2}\left(\frac{m}{m_\alpha}\right)^{1/2}\int_{-\infty}^{+\infty} h_\alpha(\boldsymbol{c}_\alpha, r)\phi^{(k)}(c_{\alpha z})e^{-c_{\alpha z}^2}\mathrm{d}c_{\alpha z} \tag{22}$$

for $k = 1,2$, where $\phi^{(1)} = c_{\alpha z}$ and $\phi^{(2)} = c_{\alpha z}^2 - 3/2$. In terms of the new function, the kinetic equation reads

$$c_{\alpha x}\frac{\partial Y_\alpha^{(k)}}{\partial r} - \frac{c_{\alpha y}}{r}\frac{\partial Y_\alpha^{(k)}}{\partial\varphi} = \omega_\alpha\sum_{\beta=1}^{3} Q_{\alpha\beta}^{(k)} - w^{(k)}\left(\frac{m}{m_\alpha}\right)^{1/2}\frac{X_\alpha}{2}, \tag{23}$$

where

$$Q_{\alpha\beta}^{(1)} = -\gamma_{\alpha\beta}Y_\alpha^{(1)} + A_{\alpha\beta} + 2\left(\frac{m}{m_\alpha}\right)^{1/2}B_{\alpha\beta}c_{\alpha x} + \frac{2}{5}D_{\alpha\beta}(c_{\alpha T}^2 - 1) \tag{24}$$

and

$$Q_{\alpha\beta}^{(2)} = -\gamma_{\alpha\beta}Y_\alpha^{(2)} + \frac{3}{5}D_{\alpha\beta}. \tag{25}$$

In this description, $c_{\alpha T}^2 = c_{\alpha x}^2 + c_{\alpha y}^2$ and $w^{(1)} = 1$, $w^{(2)} = 0$. The macroscopic moments are calculated according to

$$u_{\alpha z} = \pi^{-1}\int_{-\infty}^{+\infty}\int_{-\infty}^{+\infty} Y_\alpha^{(1)}e^{-c_{\alpha T}^2}\mathrm{d}c_{\alpha x}\mathrm{d}c_{\alpha y}, \tag{26}$$

$$p_{\alpha xz} = \pi^{-1}\left(\frac{m_\alpha}{m}\right)^{1/2}\int_{-\infty}^{+\infty}\int_{-\infty}^{+\infty} Y_\alpha^{(1)}c_{\alpha x}e^{-c_{\alpha T}^2}\mathrm{d}c_{\alpha x}\mathrm{d}c_{\alpha y}, \tag{27}$$

$$q_{\alpha z} = \pi^{-1}\int_{-\infty}^{+\infty}\int_{-\infty}^{+\infty}\left[Y_\alpha^{(1)}(c_{\alpha T}^2 - 1) + Y_\alpha^{(2)}\right]e^{-c_{\alpha T}^2}\mathrm{d}c_{\alpha x}\mathrm{d}c_{\alpha y}. \tag{28}$$

The boundary condition for the reduced distribution function at the tube wall can be written by $Y_\alpha^{(k)}(c_{\alpha x}, c_{\alpha y}, 1) = 0$ for $k = 1,2$ and $c_{\alpha x} < 0$.

Equations (23) and (26)–(28) are solved by the discrete velocity method. The radial coordinate of the velocity space is represented by a Gauss–Legendre quadrature $c_\alpha = \xi_i$, $1\le i\le K$. The polar coordinate of the same space is discretized by $\varphi = \varphi_j = (j - 0.5)\pi/L + \pi$, $1\le j\le L$. Finally, the radial coordinate is discretized as $r = r_k = (k-1)/(M-1)$, $1\le k\le M$. The spatial derivatives in Eq. (23) are approximated by finite differences, and the integrals in Eqs. (26)–(28) are calculated by the quadrature. The kinetic equation is solved by an iterative manner. At a given iteration step, by assuming the macroscopic moments at the right-hand side of Eq. (23), this equation is integrated along the particle trajectories in order

to yield the reduced distribution function. By using these functions, the macroscopic moments in the next iteration stage are calculated on the basis of Eqs. (26)–(28). The new moments are inserted into Eq. (23) again, and the whole iteration is repeated until a desirable convergence is not reached. A convergence parameter ϵ is defined as the maximum of the sum of the absolute relative differences in the velocities of the three species between two subsequent iteration stages. The iteration is terminated when $\epsilon < 1e{-}7$. The complete solution method for the tube geometry is described in Szalmas (2013b). That treatment has been adjusted for the present three-component mixture. Interested reader may consult with that paper for more detail about the numerical approach.

3.4 Pressure-driven flow in a tube

As an application of the approach, the flow of the ternary mixture subject to a global pressure difference in a long tube is calculated. In this context, the goal is to deduce the flow rates of the species and the distributions of the mole fractions and the pressure along the axis of the tube. This calculation can be done by the consideration of the mass conservation for each component. However, unlike previous approaches in the present work, the more general time-dependent diffusion problem is solved to deduce the above-mentioned quantities. The time-dependent treatment is found to be more powerful numerically than the steady calculation.

It is supposed that the flow is through the tube between two large reservoirs having constant inlet (A) and outlet (B) mole fractions and pressures as C_α^A, C_α^B and P^A, P^B. The dimensionless flow rates are introduced according to

$$J_\alpha = J'_\alpha \frac{2L}{n^A v_0 A R}, \tag{29}$$

where n^A is the total number density at the inlet of the tube. By using the dimensionless kinetic coefficients, the dimensionless flow rate can be written by

$$J_\alpha = -\sum_{\beta=1}^{3} L_{\alpha\beta} \frac{n_\alpha}{n^A} \frac{\partial n_\beta}{\partial \hat{z}} \frac{1}{n_\beta}, \tag{30}$$

where $\hat{z} = z'/L$ is the non-dimensional coordinate along the axis of the tube. If the flow is quasi-steady, i.e., the time-scale of the macroscopic processes is much larger than that of the microscopic ones, one can write that

$$\frac{\partial n_\alpha}{\partial t'} A = -\frac{\partial J'_\alpha}{\partial z'}, \tag{31}$$

where t' is the time variable. This equation by using Eq. (30) can be rewritten in dimensionless form as

$$\frac{\partial \zeta_\alpha}{\partial t} = \frac{1}{2} \sum_{\beta=1}^{3} \left[\frac{\partial}{\partial \hat{z}} \left(L_{\alpha\beta} \frac{\zeta_\alpha}{\zeta_\beta} \right) \frac{\partial \zeta_\beta}{\partial \hat{z}} + L_{\alpha\beta} \frac{\zeta_\alpha}{\zeta_\beta} \frac{\partial^2 \zeta_\beta}{\partial \hat{z}^2} \right], \tag{32}$$

where $\zeta_\alpha = \zeta_\alpha(t, \hat{z}) = n_\alpha(t, \hat{z})/n^A$ and $t = t' v_0 R/L^2$ are the normalized density and the dimensionless time. The goal is to obtain a solution for the steady-state problem. Equation (32) is supplemented with the following boundary condition

$$\zeta_\alpha(t, 0) = C_\alpha^A, \quad \zeta_\alpha(t, 1) = C_\alpha^B \frac{P^B}{P^A}. \tag{33}$$

Equation (32) is solved by the finite difference method. The temporal and spatial coordinates are discretized by $t = i\Delta t$, $i \geq 0$ and $\hat{z} = (j-1)\Delta\hat{z}$, $\Delta\hat{z} = 1/(N-1)$, $1 \leq j \leq N$. Here, Δt and $\Delta\hat{z}$ denote the time and space steps. The dimensionless density and kinetic coefficients are represented by $\zeta_\alpha(t, \hat{z}) = \zeta_\alpha[i,j]$ and $L_{\alpha\beta}(t, \hat{z}) = L_{\alpha\beta}[i,j]$. The stable solution of diffusion equations requires implicit treatments. In the present work, the following implicit scheme is used

$$\begin{aligned}
&\zeta_\alpha[i+1,j] \left[1 + \frac{\Delta t}{\Delta \hat{z}^2} \sum_{\beta=1}^{3} L_{\alpha\beta}[i,j] \right] \\
&= \zeta_\alpha[i,j] + \frac{\Delta t}{8\Delta \hat{z}^2} \sum_{\beta=1}^{3} \left[\left(L_{\alpha\beta}[i,j+1] \frac{\zeta_\alpha[i,j+1]}{\zeta_\beta[i,j+1]} \right.\right. \\
&\quad \left. - L_{\alpha\beta}[i,j-1] \frac{\zeta_\alpha[i,j-1]}{\zeta_\beta[i,j-1]} \right) \\
&\quad \times (\zeta_\beta[i,j+1] - \zeta_\beta[i,j-1]) \\
&\quad \left. + 4 L_{\alpha\beta}[i,j] \frac{\zeta_\alpha[i,j]}{\zeta_\beta[i,j]} (\zeta_\beta[i,j+1] + \zeta_\beta[i,j-1]) \right].
\end{aligned} \tag{34}$$

It is noted that $L_{\alpha\beta}[i,j]$ depends on the local mole fractions and the pressure, which can be deduced from $\zeta_\alpha[i,j]$. For this reason, the correct viscosity as an input parameter as defined in Sect. 3.2 is used. Equation (34) is subject to the boundary conditions of Eq. (33). By assuming an initial state when $\zeta_\alpha[0,j]$ is taken to be a linear function between the inlet and outlet values, Eq. (34) is iteratively solved for obtaining the final steady state. The simulation is considered converged if the maximum of the relative difference in the local flow rates between two subsequent iteration steps is less than $(1e{-}10)/\Delta t$.

A separate code to obtain steady-state results for the pressure-driven flow of the ternary mixture on the basis of the treatment in Szalmas and Valougeorgis (2010) has also been developed. The steady-state results provided by the two codes have been compared to each other at inlet rarefaction parameter $\delta^A = 1$ for a test composition of He–Ar–Xe. The results agree with four-figure accuracy and plus–minus one in the fifth figure in terms of the dimensionless flow rates. Such an agreement validates the present method.

4 Results

4.1 Local flow problem

The kinetic coefficients are calculated for He–Ar–Xe mixture at various values of the local rarefaction parameter and mole fractions. The species of the mixture are numbered in the same order. Therefore, He, Ar, Xe are the first, second, and third components. The mass ratios of these gases are $m_1/m_2 = 4.0026/39.948$ and $m_1/m_3 = 4.0026/131.29$. The collision frequencies have been calculated on the basis of either the realistic potential (Exp) at temperature $T = 300\,K$ (Kestin et al. 1984) or the hard-sphere gas (HS). In this latter case, the diameter ratios are $d_2/d_1 = 1.665$, $d_3/d_1 = 2.226$, and the used expressions of the Chapman–Cowling integrals are given in Naris et al. (2004b) for example. Since there are three components of the mixture, the whole set of collision frequencies are deduced from the binary pair collision frequencies. Since there are only binary interactions in the gas, this treatment is sufficient. It is noted that all results presented in Sect. 4 are computed with the realistic potential, expect Table 4, which shows results for the hard-sphere gas. Nevertheless, it is expected that the realistic potential provides more reliable data than the hard-sphere interaction. In the discrete velocity solution, the following parameters are used $K = [16, 80]$ for $\delta > 2, \delta \leq 2$, respectively, and $L = 160$, $M = 301$. Before doing the actual calculation, the present McCormack solver has been validated for binary He–Ar and He–Xe mixtures at $C_1 = 0.5$ and $\delta = [0.1, 1, 10]$ with hard-sphere interaction. The corresponding kinetic coefficients of the present approach and those calculated by the discrete velocity method of Szalmas (2013b) agree with five-figure accuracy and plus–minus one in the sixth figure. In addition, the flow rates for pressure-driven single gas flows have been calculated by setting $X_1 = 1, X_2 = X_3 = 0$ and $C_1 = 1, C_2 = C_3 = 0$ at $\delta = [0.1, 1, 10, 20, 40]$. In this case, the McCormack equation results into the Shakov (S) model. L_{11} is compared to the corresponding flow rates calculated by the method in Szalmas (2013b) and those results (Q_P) given in Sharipov (1996). In the former case, the flow rates agree with five-figure accuracy, while in the latter case, the absolute relative difference between L_{11} and Q_P is less than $8e{-}4$.

Table 1 shows the scaled dimensionless kinetic coefficients $C_\alpha L_{\alpha\beta}$ for He–Ar–Xe in the whole range of gaseous rarefaction at mole fractions $C_1 = 0.5$ and $C_2 = 0.2$. For this scaled coefficient, the Onsager relation is also hold; hence, only six elements of the coefficient are shown. It is noted that the Onsager relation is found true for six-figure accuracy in the numerical simulation in all cases. The scaled dimensionless kinetic coefficients provide the dimensionless flow rate for the three driving terms, whereas $L_{\alpha\beta}$ describes the mean value of the velocity of the components. As it can be seen in the table, the main coefficients $C_\alpha L_{\alpha\alpha}$ show the Knudsen minimum in terms of the rarefaction parameter. They start to decrease in the hydrodynamic region as approaching the transition region, where they take a minimum, and increase as the rarefaction approaches the free molecular limit. These coefficients describe the flow rate of those components that are accelerated. In the hydrodynamic limit, $C_1L_{11} > C_3L_{33} > C_2L_{22}$ since $C_1 > C_3 > C_2$. However, as the rarefaction is increased, the relation of C_3L_{33} and C_2L_{22} changes: $C_3L_{33} < C_2L_{22}$ for $\delta \leq 0.6$. This can be explained by the fact that as the rarefaction is increased, the components become more independent and the lighter species tends to travel faster than the heavier one. The cross coefficients $C_\alpha L_{\alpha\beta}$, $\alpha \neq \beta$ decrease with increasing rarefaction. In the hydrodynamic limit, there are more frequent intermolecular collisions resulting into finite cross coefficients, which might be in the same order as $C_\alpha L_{\alpha\alpha}$. However, as the rarefaction is increased, there are fewer molecular collisions; hence, the cross coefficients tend to zero as $\delta \to 0$. The last row of the table shows the global kinetic coefficient L_{PP} for a pressure-driven flow $X_1 = X_2 = X_3 = -1$. For the ternary gas, it is defined as $L_{\mathrm{PP}} = \sum_\alpha C_\alpha L_{\alpha\alpha}$. This coefficient provides the dimensionless total flow rate for a pressure-driven flow. As it can be seen, L_{PP} exhibits the Knudsen minimum as all $C_\alpha L_{\alpha\alpha}$ do so. It takes its minimum in the transition region at $\delta = 5$ in the table. Finally, it is mentioned that for all cases in Table 1, the free molecular kinetic coefficients have also been calculated. These values agree with the corresponding analytical results, Eq. (16), with five-figure accuracy.

Tables 2 and 3 present the scaled kinetic coefficients for He–Ar–Xe versus C_1 and C_2, respectively, but with a fixed another mole fraction at rarefaction parameter $\delta = 1$ in order to examine the influence of the mole fractions. In Table 2, C_1L_{11} and C_1L_{12} monotonically increase, but C_3L_{33} and C_2L_{23} monotonically decrease, with increasing C_1 due to the increasing amount of He compared to Xe. In the limiting cases, $C_1L_{11} = C_1L_{12} = 0$ at $C_1 = 0$ and $C_3L_{33} = C_2L_{23} = 0$ at $C_1 = 0.8$. C_1L_{13} is zero in these two limiting cases, but it has a maximum at $C_1 = 0.4$. This can be explained by the fact that if $C_1 = 0$, there is no He and $C_1L_{13} = 0$; on the other hand, if $C_1 = 0.8$, there is no Xe and $L_{13} = 0$. Since the kinetic coefficients are positive, a maximum for C_1L_{13} is presented at a middle value of C_1. C_2L_{22} monotonically decreases with increasing C_1. This latter behavior is caused by the dependence of the viscosity on the mole fractions. Since the viscosity of Xe is larger than those of He and Ar, if the amount of Xe is increased, then the total pressure should be lowered to simulate the same rarefaction parameter $\delta = 1$. As a consequence, the

Table 1 Scaled dimensionless kinetic coefficients $C_\alpha L_{\alpha\beta}$ for He–Ar–Xe mixture at $C_1 = 0.5$ and $C_2 = 0.2$ versus rarefaction parameter

δ	C_1L_{11}	C_2L_{22}	C_3L_{33}	C_1L_{12}	C_1L_{13}	C_2L_{23}	L_{PP}
0.05	2.483	3.099e−1	2.604e−1	6.400e−3	7.216e−3	4.521e−3	3.053
0.1	2.388	2.956e−1	2.523e−1	1.197e−2	1.364e−2	8.366e−3	2.936
0.2	2.252	2.752e−1	2.423e−1	2.177e−2	2.528e−2	1.500e−2	2.769
0.4	2.063	2.482e−1	2.312e−1	3.827e−2	4.586e−2	2.593e−2	2.542
0.6	1.926	2.295e−1	2.251e−1	5.230e−2	6.431e−2	3.504e−2	2.380
0.8	1.817	2.153e−1	2.215e−1	6.474e−2	8.134e−2	4.301e−2	2.254
1	1.728	2.041e−1	2.194e−1	7.603e−2	9.728e−2	5.016e−2	2.152
1.5	1.560	1.843e−1	2.182e−1	1.008e−1	1.336e−1	6.560e−2	1.962
2	1.442	1.717e−1	2.205e−1	1.223e−1	1.662e−1	7.872e−2	1.834
2.5	1.357	1.636e−1	2.249e−1	1.417e−1	1.960e−1	9.038e−2	1.745
3	1.295	1.585e−1	2.307e−1	1.596e−1	2.239e−1	1.011e−1	1.684
4	1.218	1.537e−1	2.450e−1	1.926e−1	2.752e−1	1.205e−1	1.617
5	1.182	1.536e−1	2.616e−1	2.231e−1	3.226e−1	1.385e−1	1.597
7	1.176	1.607e−1	2.987e−1	2.802e−1	4.107e−1	1.720e−1	1.636
10	1.253	1.799e−1	3.593e−1	3.611e−1	5.344e−1	2.197e−1	1.792
15	1.469	2.208e−1	4.657e−1	4.909e−1	7.313e−1	2.968e−1	2.156
20	1.731	2.660e−1	5.749e−1	6.185e−1	9.238e−1	3.728e−1	2.572
30	2.303	3.610e−1	7.963e−1	8.710e−1	1.304	5.239e−1	3.461
40	2.901	4.585e−1	1.020	1.122	1.681	6.744e−1	4.379

Table 2 Scaled dimensionless kinetic coefficients $C_\alpha L_{\alpha\beta}$ for He–Ar–Xe mixture at $C_2 = 0.2$ and $\delta = 1$ versus C_1

C_1	C_1L_{11}	C_2L_{22}	C_3L_{33}	C_1L_{12}	C_1L_{13}	C_2L_{23}
0	0.0	2.737e−1	1.025	0.0	0.0	1.211e-1
0.1	4.418e−1	2.625e−1	8.295e−1	1.389e−2	4.192e−2	1.081e−1
0.2	8.436e−1	2.503e−1	6.498e−1	2.841e−2	7.332e−2	9.455e−2
0.3	1.199	2.368e−1	4.872e−1	4.362e−2	9.358e−2	8.047e−2
0.4	1.498	2.216e−1	3.432e−1	5.953e−2	1.019e−1	6.571e−2
0.5	1.728	2.041e−1	2.194e−1	7.603e−2	9.728e−2	5.016e−2
0.6	1.865	1.831e−1	1.183e−1	9.259e−2	7.869e−2	3.376e−2
0.7	1.862	1.560e−1	4.337e−2	1.074e−1	4.545e−2	1.665e−2
0.8	1.583	1.151e−1	0.0	1.138e−1	0.0	0.0

Table 3 Scaled dimensionless kinetic coefficients $C_\alpha L_{\alpha\beta}$ for He–Ar–Xe mixture at $C_1 = 0.5$ and $\delta = 1$ versus C_2

C_2	C_1L_{11}	C_2L_{22}	C_3L_{33}	C_1L_{12}	C_1L_{13}	C_2L_{23}
0	2.034	0.0	4.897e−1	0.0	1.603e−1	0.0
0.1	1.887	1.010e−1	3.431e−1	3.789e−2	1.292e−1	3.351e−2
0.2	1.728	2.041e−1	2.194e−−1	7.603e−2	9.728e−2	5.016e−2
0.3	1.555	3.062e−1	1.200e−1	1.136e−1	6.467e−2	4.969e−2
0.4	1.361	4.018e−1	4.628e−2	1.492e−1	3.190e−2	3.241e−2
0.5	1.137	4.794e−1	0.0	1.801e−1	0.0	0.0

experiment shifts toward the free molecular region if C_1 is decreased; hence, a larger L_{22} is obtained. Table 3 shows the dependence of $C_\alpha L_{\alpha\beta}$ on C_2. C_2L_{22} and C_1L_{12} monotonically increase, but C_3L_{33} and C_1L_{13} monotonically decrease, if C_2 is increased due to the increasing fraction of Ar compared to Xe. On the other hand, C_2L_{23} is zero at the limiting values $C_2 = [0, 0.5]$, but it has a maximum at $C_2 = 0.2$. Finally, it can be seen that C_1L_{11} monotonically decreases with increasing C_2. These phenomena can be explained by the same way as for Table 2 but with interchanging species $1, 2$.

Table 4 shows the scaled kinetic coefficients calculated by the hard-sphere model versus the rarefaction parameter for He–Ar–Xe at $C_1 = 0.5$ and $C_2 = 0.2$. This table is

Table 4 Scaled dimensionless kinetic coefficients $C_\alpha L_{\alpha\beta}$ computed with hard-sphere potential for He–Ar–Xe mixture at $C_1 = 0.5$ and $C_2 = 0.2$ versus rarefaction parameter

δ	C_1L_{11}	C_2L_{22}	C_3L_{33}	C_1L_{12}	C_1L_{13}	C_2L_{23}	L_{PP}
0.05	2.473	3.101e−1	2.599e−1	6.887e−3	8.631e−3	4.460e−3	3.043
0.1	2.372	2.959e−1	2.516e−1	1.288e−2	1.622e−2	8.276e−3	2.919
0.4	2.019	2.481e−1	2.289e−1	4.094e−2	5.310e−2	2.587e−2	2.496
1	1.661	2.032e−1	2.158e−1	8.042e−2	1.086e−1	5.032e−2	2.080
2	1.368	1.701e−1	2.163e−1	1.275e−1	1.788e−1	7.899e−2	1.755
5	1.126	1.521e−1	2.580e−1	2.274e−1	3.325e−1	1.386e−1	1.536
10	1.218	1.788e−1	3.568e−1	3.638e−1	5.405e−1	2.197e−1	1.754
40	2.891	4.581e−1	1.019	1.123	1.683	6.742e−1	4.367

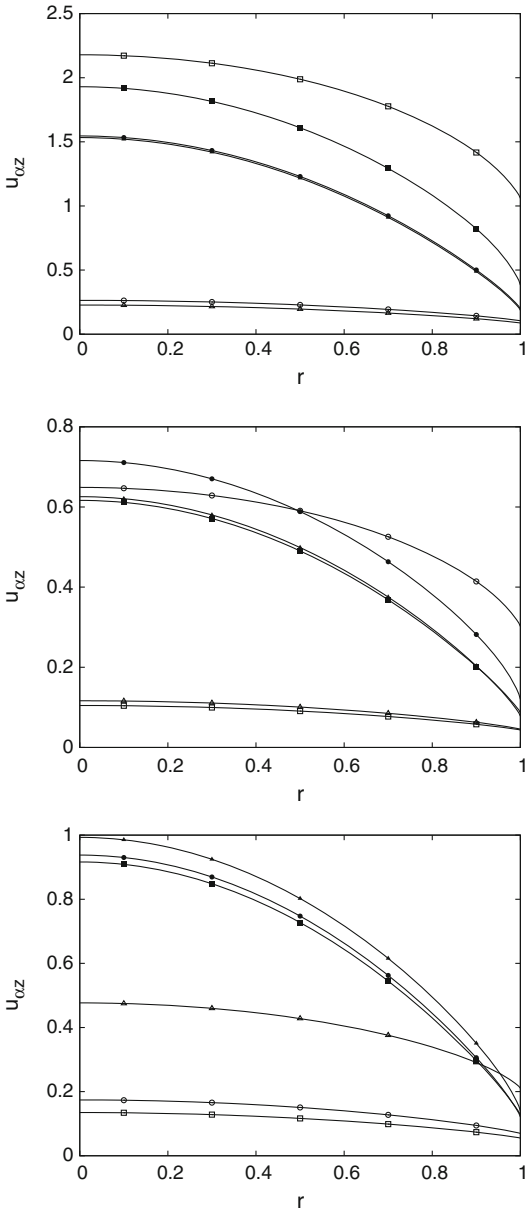

Fig. 1 Velocity profiles for He–Ar–Xe mixture at $C_1 = 0.5, C_2 = 0.2$ and $\delta = [1, 10]$ for $X_\alpha = [-1, 0, 0]$ (*top*) $X_\alpha = [0, -1, 0]$ (*center*) and $X_\alpha = [0, 0, -1]$ (*bottom*). *Squares*, *circles,* and *triangles* represent the first, second, and third species, respectively. *Empty* and*filled symbols* stand for $\delta = [1, 10]$

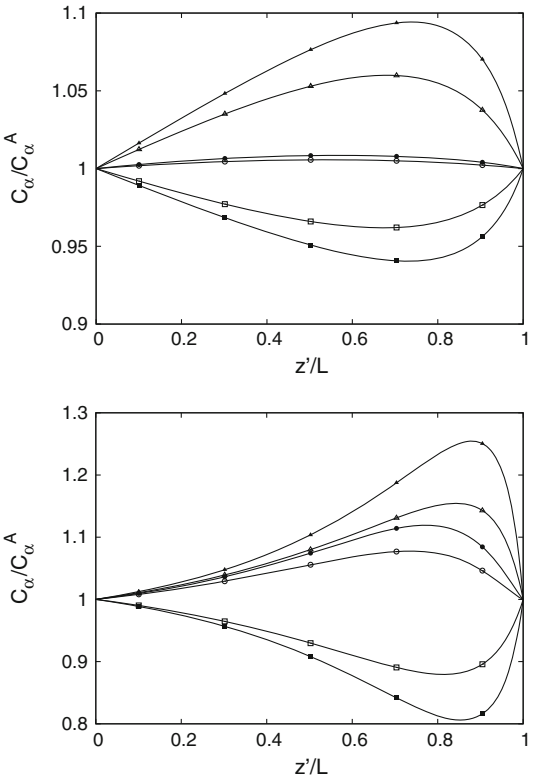

Fig. 2 Distributions of the normalized mole fractions for He–Ar–Xe mixture at $\delta^A = 1$ (*top*) and $\delta^A = 10$ (*bottom*). *Squares*, *circles,* and *triangles* represent the first, second, and third species, respectively. *Empty* and*filled symbols* stand for $\Pi = [4, 7]$

given in the same scenario as Table 1. In Table 4, the influence of the intermolecular interaction can be seen. The main coefficients $C_\alpha L_{\alpha\alpha}$ are nearly the same as those in Table 1 in the hydrodynamic and free molecular limits. In the former case, the diffusion is negligible; hence, the single gas assumption gives a good approximation of the flow. Since the hard-sphere diameters are determined on the basis of the viscosity, the result is not sensitive to the intermolecular potential. The same can be said about the free molecular limit, where there are no collisions. The highest absolute relative difference, $|L_{\alpha\alpha}^{(HS)}/L_{\alpha\alpha}^{(Exp)} - 1|$, is 5.1 %, which occurs at $\delta = 2$ for L_{11}. However, the cross

Table 5 Dimensionless flow rates for pressure-driven flow of He–Ar–Xe mixture versus pressure ratio for $\delta^A = 1$ (top) and $\delta^A = 10$ (bottom)

Π	J_1	J_2	J_3	J_{1a}	J_{2a}	J_{3a}
2	9.948e−1	1.614e−1	1.720e−1	9.547e−1	1.647e−1	1.821e−1
3	1.354	2.146e−1	2.257e−1	1.275	2.194e−1	2.422e−1
4	1.544	2.415e−1	2.524e−1	1.435	2.467e−1	2.722e−1
5	1.661	2.579e−1	2.685e−1	1.531	2.631e−1	2.901e−1
6	1.741	2.690e−1	2.794e−1	1.595	2.740e−1	3.020e−1
7	1.799	2.771e−1	2.872e−1	1.641	2.818e−1	3.106e−1
2	9.385e−1	3.234e−1	4.733e−1	1.061	3.741e−1	5.470e−1
3	1.192	4.096e−1	5.995e−1	1.410	4.961e−1	7.251e−1
4	1.310	4.497e−1	6.583e−1	1.583	5.566e−1	8.133e−1
5	1.379	4.732e−1	6.927e−1	1.686	5.927e−1	8.660e−1
6	1.425	4.887e−1	7.154e−1	1.755	6.167e−1	9.010e−1
7	1.457	4.998e−1	7.316e−1	1.804	6.338e−1	9.260e−1

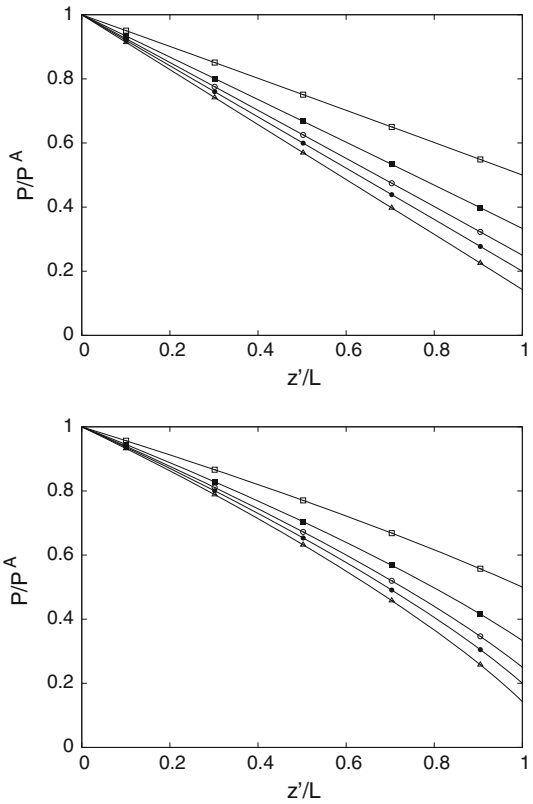

Fig. 3 Distribution of the normalized pressure for He–Ar–Xe mixture at $\delta^A = 1$ (*top*) and $\delta^A = 10$ (*bottom*). *Empty* and *filled squares*, *empty* and *filled circles*, and *empty triangle* stand for $\Pi = [2, 3, 4, 5, 7]$, respectively

coefficients $L_{\alpha\beta}, \alpha \neq \beta$, which describe diffusion, are more sensitive to the intermolecular interactions. The maximum of the absolute relative difference in the cross coefficients between the two approaches is 20 % for L_{31} at $\delta = 0.05$. The results indicate that when diffusion effects play an important role, care must be taken to chose the intermolecular potential well.

In Fig. 1, the dimensionless velocity profile is plotted for He–Ar–Xe at $C_1 = 0.5$, $C_2 = 0.2$ and $\delta = [1, 10]$ for the three types of flow when one of the components of X_α is taken to be minus one and the another two components are zero. It can be seen that the velocity profile is parabolic-like in all cases. $u_{\alpha z}$ is the largest for that component, which is accelerated, and the another two $u_{\alpha z}$ are smaller. The difference between the largest velocity and the another two ones increases with increasing rarefaction since the different species become more and more independent if the rarefaction is increased. It can also be seen that the velocity profiles of those species, which are not accelerated, are relatively close to each other.

4.2 Global pressure-driven flow

The flows of He–Ar–Xe mixture driven by pressure difference through a long tube are examined. The inlet and outlet mole fractions are fixed at $C_1^A = C_1^B = 0.5$ and $C_2^A = C_2^B = 0.2$. The dimensionless flow rates and the distributions of the pressure and the mole fractions are calculated at different inlet rarefaction parameter δ^A and pressure ratio $\Pi = P^A/P^B$ by using the methodology of Sect. 3.4. The numerical parameters are $N = 200$ and $\Delta t = 1$. The scope of the simulations is to obtain steady-state results. The larger time step, which can only be used in implicit schemes, provides faster convergence. The kinetic coefficients $L_{\alpha\beta}$ are precomputed in a wide range of gaseous rarefaction and at numerous values of the mole fractions to form a database. Then, the integration in Eq. (34) is carried out. The local values of the kinetic coefficients in Eq. (34) are deduced by using a linear interpolation of the values in the database.

Table 5 presents the dimensionless flow rates of the components J_α. As it can be seen, they increase with increasing pressure ratio, and the relation $J_1 > J_3 > J_2$ is

hold in all cases. It is worth determining the ratio J_α/J, where $J = \sum_\alpha J_\alpha$. On the basis of the results, it can be deduced that J_α/J deviates from the ideal value of C_α^A, which would be present in the strict hydrodynamic limit. This indicates that the mixture cannot be modeled as a single gas at finite rarefaction. The flow rate $J_{\alpha a}$ computed with a constant mean rarefaction parameter $\delta^0 = (\delta^A + \delta^B)/2$ and inlet mole fractions C_α^A in the dimensionless kinetic coefficients $L_{\alpha\beta}$ is also shown. $J_{\alpha a}$ can significantly differ from J_α. The maximum absolute relative difference $|J_{\alpha a}/J_\alpha - 1|$ is 8.8 % and 27 % for $\delta^A = 1$ and 10, respectively.

Figures 2 and 3 show the distributions of the normalized mole fractions and pressure, respectively, for the mixture at $\delta^A = [1, 10]$ and various values of the pressure ratio. In Fig. 2, it can be seen that the mole fractions are non-uniform. In the case of He, the mole fraction decreases in the first part of the channel, takes a minimum somewhere in the second part, and starts to increase to reach the outlet value. In the case of Ar and Xe, a mirrored behavior is shown. The results indicate that the gas separates in the tube. The non-uniformity of the mole fraction increases with increasing pressure ratio, and it is larger for $\delta^A = 10$ than 1. Generally, the mole fraction of Ar, of which mass is most close to the mean mass of the mixture, is most uniform. Figure 3 shows that the pressure monotonically decreases along the axis of the channel. At $\delta^A = 1$, the pressure profile is more linear than at $\delta^A = 10$. The complete linear pressure distribution refers to the free molecular limit, while the pressure profile is more nonlinear as approaching the hydrodynamic limit.

5 Conclusion

In this paper, a methodology has been presented to compute isothermal flows of rarefied three-component gaseous mixtures in long tubes. The mixture is described by the McCormack linearized kinetic model, which is solved by the discrete velocity method. An additional method has also been developed to determine the flow of the mixture subject to a global pressure difference through the tube. The local flow problem has been solved for He–Ar–Xe mixture in a wide range of the gaseous rarefaction and various values of the mole fractions. The kinetic coefficients are tabulated for these cases, and demonstrative velocity profiles are shown. Pressure-driven flows of He–Ar–Xe mixture in a long tube have also been calculated. The flow rates and the distributions of the mole fractions and the pressure are presented. The ternary mixture exhibits the gaseous separation. The distributions of the mole fractions are non-uniform. The developed methodology can be useful in the proper determination of the flow of three-component gaseous mixtures in a wide range of gaseous rarefaction.

Acknowledgments This research obtained financial support from the Marie Curie Action COFUND of the European Community's Seventh Framework Programme for Research and Technological Development (2007–2013) in the Project BREMEN TRAC.

References

Andries P, Aoki K, Perthame B (2002) A consistent BGK-type model for gas mixtures. J Stat Phys 106:993–1018

Cercignani C (2006) Slow rarefied flows: theory and applications to micro-electro-mechanical systems. Birkhauser Verlag, Basel, Boston, Berlin

Jousten K (ed) (2008) Handbook of vacuum technology. Wiley-VCN, Berlin

Kandlikar SG, Garimella S et al (2006) Heat transfer and fluid flow in minichannels and microchannels. Elsevier, Oxford

Kestin J, Knierim K, Mason EA, Najafi B, Ro ST, Waldman M (1984) Equilibrium and transport properties of the noble gases and their mixture at low densities. J Phys Chem Ref Data 13:229–303

Li D (ed) (2008) Encyclopedia of Microfluidics and nanofluidics. Springer, New York

McCormack FJ (1973) Construction of linearized kinetic models for gaseous mixtures and molecular gases. Phys Fluids 16:2095–2105

Morse TF (1964) Kinetic model equations for a gas mixture. Phys Fluids 7:2012–2013

Naris S, Valougeorgis D, Sharipov F, Kalempa D (2004a) Discrete velocity modelling of gaseous mixture flows in MEMS. Superlattices Microstruct 35:629–643

Naris S, Valougeorgis D, Kalempa D, Sharipov F (2004b) Gaseous mixture flow between two parallel plates in the whole range of the gas rarefaction. Physica A 336:294–318

Sharipov F (1994) Onsager-Casimir reciprocity relations for open gaseous systems at arbitrary rarefaction. III. Theory and its application for gaseous mixtures. Physica A 209:457–476

Sharipov F (1996) Rarefied gas flow through a long tube at any temperature ratio. J Vac Sci Technol A 14:2627–2635

Sharipov F (2013) Gaseous mixtures in vacuum systems and microfluidics. J Vac Sci Technol A 31:050806

Sharipov F, Kalempa D (2002) Gaseous mixture flow through a long tube at arbitrary Knudsen numbers. J Vac Sci Technol A 20:814–822

Sharipov F, Kalempa D (2005) Separation phenomena for gaseous mixture flowing through a long tube into vacuum. Phys Fluids 17:127102

Sirovich L (1962) Kinetic modeling of gas mixtures. Phys Fluids 5:908–918

Szalmas L (2010) Flows of rarefied gaseous mixtures in networks of long channels. Microfluid Nanofluid 9:471–487

Szalmas L (2012) Variance-reduced DSMC for binary gas flows as defined by the McCormack kinetic model. J Comput Phys 231:3723–3738

Szalmas L (2013a) Accelerated discrete velocity method for axial-symmetric flows of gaseous mixtures as defined by the McCormack kinetic model. Comput Phys Commun 184:2430–2437

Szalmas L (2013b) Variance-reduced DSMC method for axial-symmetric flows of gaseous mixtures. Comput Fluids 74:58–65

Szalmas L, Valougeorgis D (2010) Rarefied gas flow of binary mixtures through long channels with triangular and trapezoidal cross sections. Microfluid Nanofluid 9:471–487

Szalmas L, Pitakarnnop J, Geoffroy S, Colin S, Valougeorgis D (2010) Comparative study between computational and experimental results for binary rarefied gas flows through long microchannels. Microfluid Nanofluid 9:1103–1114